Microwave enhanced demulsification of metal ion extraction emulsions: From permittivity modeling to proof of concept for solvent extraction processes

C. Cerino, H. Roussel, Lionel Estel, Sophie Charton, Isabelle Polaert

Chemical Engineering Research and Design 207 (2024) 331–344

Contents lists available at ScienceDirect

Chemical Engineering Research and Design

journal homepage: www.elsevier.com/locate/cherd

Microwave enhanced demulsification of metal ion extraction emulsions: From permittivity modeling to proof of concept for solvent extraction processes

C. Cerino [a,b], H. Roussel [b,*], L. Estel [a], S. Charton [b], I. Polaert [a,*]

[a] INSA Rouen Normandie, Univ Rouen Normandie, Normandie Université, LSPC UR 4704, Rouen F-76000, France
[b] CEA, DES, ISEC, DMRC, Univ. Montpellier, Marcoule, France

ARTICLE INFO

Keywords:
Liquid-liquid separation
Demulsification
Microwave
Solvent extraction

ABSTRACT

The demulsification by microwaves of liquid-liquid systems for metal recycling was experimentally and numerically investigated. Strongly ionic aqueous phases with high conductivities and typical organic phases, both representative of industrial ones, were used. Experimental microwave demulsification was achieved in both the W/O and O/W systems at the laboratory scale showing the rapidity and the efficiency of the process. The dielectric properties of these representative emulsions were measured and modeled using the permittivities measured in the separate phases and the phase fractions. Taking into account the direction of the emulsion, permittivities were predicted over a wide range of frequencies, along with microwave penetration depths in the whole range of phase fractions. Numerical simulations of the electric field distribution and penetration depths calculations at several frequencies demonstrated that microwave heating is relevant and possible in both W/O and O/W dense packed emulsions, which should rapidly lead to demulsification, including on a large industrial scale.

1. Introduction

The supply of strategic elements is a major challenge for securing the decarbonation of transports and energy, making their recycling a major challenge. There is hence an urgent and crucial need for the development of new processes and technology. The low energy requirements of solvent extraction make it an attractive approach for separation operations in the chemical and nuclear industry. Liquid–liquid extraction exploits differences in solubility to exchange compounds of interest between two immiscible phases. To enhance the mass transfer, liquid–liquid dispersions are created where one phase is dispersed as droplets in the second. Once mass transfer is completed, the phases need to be separated, by coalescence.

Frequently, due to excessive agitation rates, an increase of viscosity, accumulation of impurities or pollutants, or a combination of these factors, the stability of the dispersion generated increases, requiring more time to achieve complete phase separation and eventually leading to the formation of “emulsions”. In this work, the term “emulsions” will be used to designate excessively stable liquid-liquid dispersions, even though diameters are of the order of a hundred microns for permittivity measurements and of a millimeter for column separation. The excessive stability of these so called emulsions can significantly affect the separation efficiency, by phase entrainment, and require a reduction in the process rate. Many solutions to this problem have been proposed over the years, as reviewed by Frising et al. (2006). Mechanical solutions can be proposed, such as the insertion of coalescence grids (Han et al., 2017) or more recently centrifugal settlers mimicking “enhanced gravity” (Baker et al., 2022). Chemical solutions such as well-chosen interfacial active species acting as demulsifiers are often incompatible with the generally complex chemical environment of metal recycling, and/or have the drawback of adding pollutants to the outputs of the process. In contrast, thermal treatment is widely employed in crude oil desalting (Vafajoo et al., 2012). Heating both phases increases their relative velocity, accelerating the hydrodynamic steps of the coalescence process, namely sedimentation and film drainage, particularly slow with viscous continuous phases. Heating also reveals to promote the formation of holes in the interfacial film trapped between the drops (Deminière et al., 1998). The positive effect on the phase separation was recently confirmed for emulsion achieved by intense mixing, as in liquid-extraction processes (Ye et al., 2023).

* Corresponding authors.
E-mail addresses: herve.roussel@cea.fr (H. Roussel), isabelle.polaert@insa-rouen.fr (I. Polaert).

https://doi.org/10.1016/j.cherd.2024.06.010
Received 20 December 2023; Received in revised form 28 May 2024; Accepted 10 June 2024
Available online 11 June 2024

Conventional heating processes, generally applied to the walls of the tank, are likely to cause significant temperature gradients in the system. Alternatively, microwave heating allows for more uniform heating in the volume. A set of guidelines for the development of microwave was proposed by Estel et al. (2017). Microwaves interact directly with the chemical system and therefore produce heating throughout the volume they pass through: the electromagnetic energy is instantaneously converted into thermal energy inside the materials (Pozar, 2012), with a conversion efficiency that depends on the dielectric properties of the system and on the electric field distribution. Microwave heating can furthermore be designed to only act in specific areas. Heating can be indirect, meaning that some fluids can be irradiated through carefully chosen walls or windows. The heating effect is very fast and easy to control by simply switching the microwave generator on and off, giving a valuable process safety advantage.

Separation intensification by microwave heating revealed encouraging results with both standard 2.45 GHz microwave radiation (Binner et al., 2013, 2014; Chan and Chen, 2002; Fang et al., 1988, 1989; Fortuny et al.,2007; Kovaleva et al., 2011), and 915 MHz (radio-frequency) waves (Ferreira et al. 2013). Except for Chan and Chen (2002), who studied solvent extraction emulsions, most of these works were dedicated to water/petroleum emulsions whose separation is greatly hampered by the presence of asphaltenes. The extraction solutions used to recover metal ions deviate significantly from those used in the oil industry. The physico-chemical characteristics (viscosity, salinity, ionicity, surface pollution, etc.) are very different, and the problem of demulsification time is much more critical in extraction processes, where production rates dictate short or even very short separation times. This is even more true in the case of column processes (agitated or pulsed), where the size of the (vertical) settling tanks requires separation times of a few minutes, and which are therefore particularly prone to clogging problems.

In order to further develop the application of microwave demulsification, a more careful consideration of some basic physical properties is required. Hence, although the results of the previously mentioned studies are encouraging, most do not report reliable data for the dielectric permittivity of the emulsions or the absorbed power, two essential parameters to optimize the microwave treatment of emulsions. The dielectric permittivity depends on the composition of the fluid, the size of the drops and the phase fractions, whereas the values reported in the literature correspond mainly to simple water-in-oil (W/O) or oil-in-water (O/W) emulsions such as lossless organic phases (*i.e.* with zero conductivity and zero permittivity imaginary part) mixed with pure or lightly ionic aqueous phases. Thus, the specific behavior under microwaves of solvents used for metal recovery is to be examined. In many cases, the drops are assumed to have the same size, and phase distributions in the dense zone are not considered. Understanding and being able to model the dielectric permittivity of such biphasic media is essential for upscaling the process and go towards an industrial design using simulation. In practical case, it is particularly important for metal ion extraction systems, involving settled emulsions with droplets in contact with each other.

The aim of this work is to investigate the applicability of microwave assisted phase separation in metal recycling by solvent extraction from laboratory to industrial scale. Strongly ionic aqueous phase and an organic phase containing a low polarity extractant molecule and a diluent will be used to specifically study representative systems of such applications. Since the goal of microwave heating in this context is to favour coalescence, we will focus on dense emulsions, *i.e.* settled emulsions in which the drops are only separated by thin films. Both O/W and W/O systems will be examined. In a first step, the microwave demulsification concept for such systems will be experimentally demonstrated in a laboratory experimental setup producing dense emulsions in an extraction column with a decantation zone. In a second step, the dielectric permittivity of representative emulsions both O/W and W/O will be measured and modeled. Finally, the values obtained will be used to simulate microwave and electric field propagation in dense-packed emulsion media to go towards the industrial design. These steps are compulsory to optimize the design of any microwave applicator.

2. Microwave propagation in 2-phase medium: theory and state of art

During microwave irradiation, the emulsion volume, composition and temperature will change. These changes will affect the absorption of microwave because of the subsequent change in permittivity of the materials. The propagation equation for the electric field in a material is given by Maxwell's equation:

$$\nabla \times \left(\mu_r^{-1} \nabla \times E\right) - k_0^2 \left(\varepsilon_r - \frac{j\sigma}{\omega \varepsilon_0}\right) E = 0 \tag{1}$$

Where $\varepsilon_r = \varepsilon_r' - j\,\varepsilon_r''$ is the relative permittivity, μ_r is the relative magnetic permeability, ε_0 and μ_0 are the free space properties, k_0 is the wave number in free space given by $k_0 = \omega\sqrt{\varepsilon_0 \mu_0}$ and σ is the electric conductivity. The materials considered here are non-magnetic so $\mu_r = 1$.

The volumetric power, p_v (W/m^3) absorbed at any location of the medium is calculated from the electric field distribution using the Poynting's theorem.

$$\langle p_v \rangle = \frac{\omega}{2} \left|\vec{E}^2\right| \varepsilon_0 \varepsilon_r'' \tag{2}$$

The wavelength (λ) and penetration depth (d_p) inside the medium can be calculated using Eqs. (3) and (4) respectively (see Pozar, 2012), where λ_0 is the wavelength in free space.

$$\lambda = \frac{\lambda_0}{\sqrt{\sqrt{\varepsilon_r'^2 + \varepsilon_r''^2}\cos\left(\frac{1}{2}\mathrm{Atan}\left(-\frac{\varepsilon_r''}{\varepsilon_r'}\right)\right)}} \tag{3}$$

$$d_p = \frac{-\lambda_0}{2\pi\sqrt{\sqrt{\varepsilon_r'^2 + \varepsilon_r''^2}\sin\left(\frac{1}{2}\mathrm{Atan}\left(-\frac{\varepsilon_r''}{\varepsilon_r'}\right)\right)}} \tag{4}$$

The penetration depth represents the length of medium through which the amplitude of an electromagnetic wave decreases to $1/e$ (about 37 %) of its initial value.

The electric field amplitude decreases exponentially with the distance traveled through the material, and the power scales with the square of the field intensity. Permittivity values are therefore very important from a process perspective because microwaves only interact with the emulsion where the field amplitude is non-zero.

The absorbed power and its distribution in the medium not only depend on the dielectric properties of the material, but also on the geometry of the microwave applicator. Dielectric properties data are extremely rare in the literature for emulsions, due to their diversity and the wide variety of phase fractions that can be produced for a given chemical system. In addition, the effect of temperature on the dielectric properties has rarely been studied in these systems despite its strong effect on demulsification. Optimizing the geometry of a microwave demulsification system for liquid-liquid extraction contactors requires detailed knowledge of the dependence of the dielectric permittivity on these properties.

It has been known since the founding work of Maxwell (1892) that the relative permittivity of emulsions and dispersions is not a simple linear combination of the permittivities of the individual components. A number of models have therefore been developed over the past century to predict the permittivity of dispersions based on the permittivity of the individual phases (ε_c for the continuous phase and ε_d for the dispersed one) and phase fractions Φ (Lichtenecker and Rother, 1931; Hanai, 1960), (Mudgett et al., 1974; Thomas et al., 1990; Erle et al., 2000). First models proposed by Maxwell, Lichtenecker and Rother are symmetrical:

switching the values for the continuous and dispersed phase in their expression (ε_c -> ε_d, ε_d -> ε_c, Φ -> $1-\Phi$), leaves the equation unchanged, meaning that it does not matter which of the two phases is defined as continuous or dispersed.

Erle et al. (2000) explained that the presence of interfaces between conducting and non-conducting phases can lead to specific polarization effects in W/O emulsions that do not arise in either of the phases separately. These effects do not occur in O/W emulsions, where the continuous phase (water) conducts electricity. Hence, any model that is symmetrical in terms of the two phases will fail to account for these effects. Wagner (1914) obtained the following expression for the complex dielectric permittivity of a dispersion by considering a sparse distribution of drops throughout the continuous medium:

$$\varepsilon_m = \varepsilon_c \frac{2\varepsilon_c + \varepsilon_d - 2\Phi(\varepsilon_c - \varepsilon_d)}{2\varepsilon_c + \varepsilon_d + \Phi(\varepsilon_c - \varepsilon_d)} \tag{5}$$

This equation has since become the standard against which other models have been compared. Since Wagner's model is only valid at low dispersed phase fractions, Hanai (1960) proposed to widen is applicability leading to the Hanai (or iterated Wagner) equation:

$$\frac{\varepsilon_m - \varepsilon_d}{\varepsilon_c - \varepsilon_d}\left(\frac{\varepsilon_c}{\varepsilon_m}\right)^{\frac{1}{3}} = 1 - \Phi \tag{6}$$

ε_m can then be estimated by identifying the roots of a well-chosen function, as shown by Thomas et al. (1990). Combining Maxwell's expression for spheres with that of Rayleigh (1892) for cylinders, Mudgett et al. (1974) proposed a more general expression:

$$\varepsilon_m = \varepsilon_c \frac{\varepsilon_d(1 + a\Phi) + \varepsilon_c a(1 - \Phi)}{\varepsilon_c(a + \Phi) + \varepsilon_d(1 - \Phi)} \tag{7}$$

With a the shape coefficient equals to 1 for elongated (cylindrical or needle-shaped) objects and 2 for spherical particles (Erle et al., 2000). In the latter case, the Fricke-Mudgett equation is identical to the Wagner equation. Whatever the value of the shape parameter, the equation remains valid for the limiting cases of $\Phi = 0$ and $\Phi = 1$.

These models have been used in several studies of emulsion structure based on permittivity measurements. Bostock et al. (1980) studied micellar solutions and microemulsions prepared with a common surfactant. They used the difference in permittivity between W/O and O/W emulsions to investigate the phase inversion as a function of temperature. Epstein's research group (Epstein et al., 1983; Foster et al., 1981) used Hanai's model and measurements in the 1–15.4 GHz range to probe the interaction between water and surfactant, estimating the number of hydrated water molecules per surfactant molecule. Sjöblom and Gestblom (1986) performed a similar study of nonionic and ionic microemulsions, focusing on interfacially-bound water and water bound to surfactant molecules and ions. These papers all demonstrate the applicability of such models for predicting emulsion permittivities for both directions of the emulsion.

3. Materials and experimental methods

3.1. Materials

The aqueous phase was generally a 1 M solution of potassium nitrate (KNO_3), or in specified cases, simply distilled water. The organic phase was either a 30 % tributylphosphate (TBP), 70 % Isane IP175 mixture, or Isane IP175 alone. Tributylphosphate is an extractant molecule used in metal recovery, and Isane IP175 is a kerosene-like mixture of branched alkanes used as a diluent, and will be called alkane from there on. In some cases, a more viscous mineral oil (Marcol 82) was used to increase the stability of the emulsions. Crystalline KNO_3 (> 99 % purity) and TBP (> 98 %) were obtained from Sigma-Aldrich, Isane IP175 from Total Energies Special Fluids, and Marcol 82 from ExxonMobil. Commercial surfactants (Triton-X100 or Tween 20 for O/W emulsions and Span 80 for W/O emulsions), purchased from Sigma Aldrich (> 99 % purity), were added in very small amounts (10^{-4} to 10^{-5} $_{vol/vol}$ in the continuous phase) when needed. Surfactant concentrations were chosen in order to stabilize emulsions for a few minutes. They were adjusted empirically by successive trials for each system. These concentrations were afterwards found to be below the critical micellar concentrations respectively equal to. $1{,}3.10^{-4}$ $_{vol/vol}$ for Triton-X100, $6{,}7.10^{-2}$ $_{vol/vol}$ for Tween 20 and not tabulated for Span 80.

3.2. Experimental microwave demulsification setup

The purpose of this set-up is to perform demulsification tests under microwave irradiation in situations where coalescence is the limiting phenomenon. The goal is therefore to create a dense emulsion zone, where the drops coalesce, and to place this zone in the path of microwave radiation. It was chosen to reproduce a vertical decanter similar to that of a pulsed column, where the continuous phase stays still and the dispersed phase is continuously fed in the form of drops and evacuated after coalescence.

Like an extraction column decanter, the device essentially consists of a simple vertical cylinder fitted with feed and withdrawal points at its two ends. It is made of glass, with an internal diameter of 25 mm and a height of 50 cm.In order to simplify the set-up and rapidly reach stable operation, the droplets are generated by letting the phase to be dispersed flow through a perforated plate. This type of set-up has the advantage of producing a monodisperse droplet population, unlike systems where dispersion is produced by agitation (Kopriwa, 2013). This point was verified by drop size measurements (see appendix A).

This technique is most commonly used for experiments in O/W mode: the perforated plate is placed at the bottom of the settler, the light phase to be dispersed is introduced under this plate, passes through it and rises, in the form of drops, through the continuous heavy phase, then coalesces and leaves the settler via a simple overflow. As our aim was to study both types of emulsion, a slightly more complex set-up was designed for W/O operation. The perforated plate is located at the top of the settler, the heavy phase to be dispersed is introduced above it, passes through it and sinks, in the form of drops, through the continuous light phase, coalesces and leaves the settler via a pipe leading back to the buffer tank. The height of the outlet pipe is used to adjust the position of the coalescence zone in the settler (by balancing the pressures in the settler and in the outlet pipe).To facilitate drop formation, the perforated plate is made of a material that is not wetted by the dispersed phase: hydrophilic material (stainless steel) in O/W mode and hydrophobic material (PEEK) in W/O mode. Both plates have 13 holes of 0.5 mm diameter evenly distributed over the cross-section of the settler.

Microwave irradiation obviously results in a rise in the temperature of the fluids. The heat generated is dissipated partly by convection/radiation at the wall and partly by the circulation of the dispersed phase. To stabilise the temperature, the dispersed phase is cooled before being re-injected into the system via a gear pump (Ismatec Masterflex) generating a smooth flow. The only variable operating parameter (for the fluid part) is therefore the flow rate of the dispersed phase, measured using a Coriolis flowmeter (Bronkhorst Mini-CoriFlow).

To apply a controlled microwave field to the decanter, a WR340 waveguide is used. It is connected via a coaxial cable to a fixed-frequency magnetron (2.45 GHz) delivering a maximum power of 300 W. The waveguide has apertures through which the decanter can pass (these apertures are equipped with chimneys surrounding the decanter to prevent wave leakage), and a window through which the coalescence zone can be observed.

The incident wave propagates through the column and is reflected by a tuning piston placed at the end of the guide. The reflected wave is superimposed over the incident wave, producing a standing wave in the guide. The reflected power is absorbed by a water charge to prevent it being returned to the magnetron. Power sensors (Agilent) mounted on directional couplers measure the incident and reflected power upstream

of the column.

The complete set-up is shown in Fig. 1.

The temperature is measured by fibre-optic sensors. These sensors are installed at various points in the dispersed phase circuit: in the buffer tank, at the column inlet and outlet, and in the coalescence zone.

The operating parameters of the system are therefore the flow rate of the dispersed phase and the irradiation power. The measured variables are the incident (Pi) and reflected (Pr) powers, the temperatures and the thickness of the dense emulsion layer.

3.3. Permittivity measurements

An Agilent N5230-A Network Analyzer was employed in reflection mode to determine both the individual phases' and emulsions' permittivities over a wide range of frequencies (500 MHz to 20 GHz) and at ambient temperature of 20–22°C. The employed "slim form" probe is an open-ended coaxial probe (outer diameter, 2.2 mm; length, 20 cm; minimum sample thickness, 5 mm).

4. Demulsification by microwave irradiation in a laboratory vertical settler

Experiments were carried out with the setup described in (3.2) to assess the effect of microwaves on coalescence. These tests were carried out for both types of emulsions: i) for O/W, TBP (30 %) – alkane (70 %) solvent dispersed in potassium nitrate 1 M solution with 2.10^{-5} (vol.) Triton-X100 as surfactant, and ii) for W/O, potassium nitrate 1 M solution dispersed in TBP (33.3 % vol.) – alkane (33.3 % vol.) – Marcol (33.3 % vol.) solvent, without surfactants.

The test procedure was as follows: the settler, initially filled with the continuous phase, is supplied with a given flow rate of the dispersed phase. The corresponding thickness of the dense emulsion layer is measured through the transparent wall (Fig. 1). The flow rate was increased in steps of 200 mL/h, from 2400 to 3600 mL/h. After each change in flow rate, we waited for the temperatures and average height of the dense emulsion to stabilize, which takes approximately 15 min, before proceeding with the measurements.

Several series of tests were carried out for each system: i) a first series without microwaves, at ambient laboratory temperature (20 – 22 °C), ii) a series under microwave irradiation at constant power, iii) a series under cyclic microwave irradiation, iv) a final series without microwaves. In the cyclic series, microwave irradiation is applied at a power twice the previous series for 20 seconds, then stopped for 20 seconds, hence providing the same average microwave power. Objective was to determine whether the effect of microwaves varies linearly with power, or whether peaks of increased power are more effective in accelerating coalescence. The aim of the final test, without microwaves, was to verify that neither the fluids properties nor the tuning of the setup has changed during the experiment.

The maximum power applied was adjusted to limit heating of the liquids. It was higher in W/O mode (100 W) than in O/W mode (50 W), because the heat can be more efficiently dissipated in the W/O configuration, by the circulation of the aqueous phase, whose heat capacity is 2.5 times higher than that of the organic phase.

The evolution of the dense emulsion height with the dispersed phase flow rate is shown in Fig. 2 and Fig. 3 for the different irradiation conditions. For the series with cyclic irradiation, we observe that the thickness fluctuates according to the fluctuations in the irradiation, only the lowest and highest values achieved are reported for each flowrate. These figures also show the temperature measured within the dense zone in the case of continuous irradiation.

As expected, the thickness of the dense emulsion increases with the dispersed phase flow rate. Above all, and despite the relatively moderate temperature rise (around +15°C), the very sensitive effect of microwave irradiation is highlighted, with a reduction in the thickness of the dense emulsion layer by a factor of 3, on average, in O/W emulsion (maximum power 50 W) and 4.5 in W/O mode (maximum power 100 W).

On the other hand, the mode of application of the microwaves does not seem to have any influence: the minimum and maximum thicknesses measured in cyclic mode always surround the thickness measured in continuous mode.

These experiments unambiguously demonstrate that microwave irradiation makes it possible to reduce a dense emulsion by 70–80 % of its initial volume in a few seconds. The resulting temperature increase essentially affects the dispersed phase and could be limited, if necessary (as for example in the case of a fluid with a low flash point), by point irradiation. Indeed, the formation time of the dense emulsion is always much longer than its collapse time.

The previous results provide proof, on the scale of the laboratory column, of efficient and rapid demulsification by microwave irradiation. Numerical simulation can make it possible to transpose this result into a more industrial dimension, by predicting the propagation of microwaves, and therefore what the distribution of energy would be in a large system. For this, modelling dielectric properties is essential in order to integrate them into Maxwell's equations.

5. Modeling of permittivity emulsions

Emulsion permittivities were first measured as a function of known phase fractions, using emulsions specifically produced in a stirred beaker. The experimental results were used to fit the best model as a function of the direction of the emulsion (W/O or O/W), the phase fraction and the individual single phase permittivities. In a second step, dense emulsions were produced, for which a thick, vertical spanning dense-packed zone exists and permittivity measurements were performed at different heights in order to determine the vertical phase fraction profile by retrofitting with the model. The two different ways of producing emulsions are fully described in Appendix B.

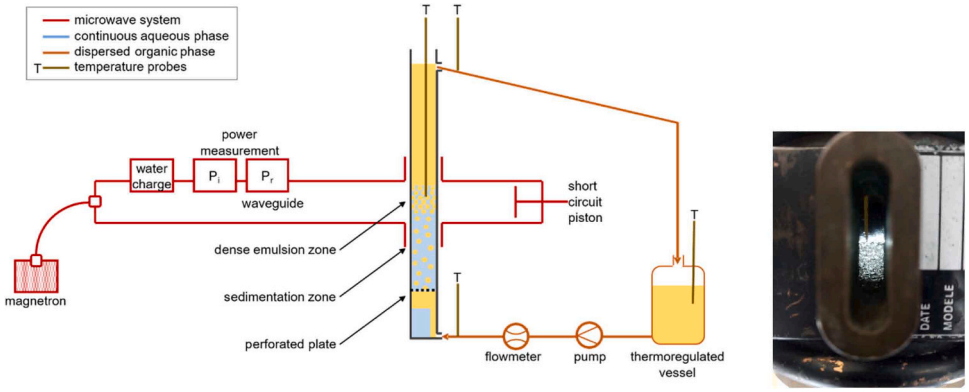

Fig. 1. Experimental setup for aqueous continuous phase mode, overall diagram (left), emulsion observation window (right).

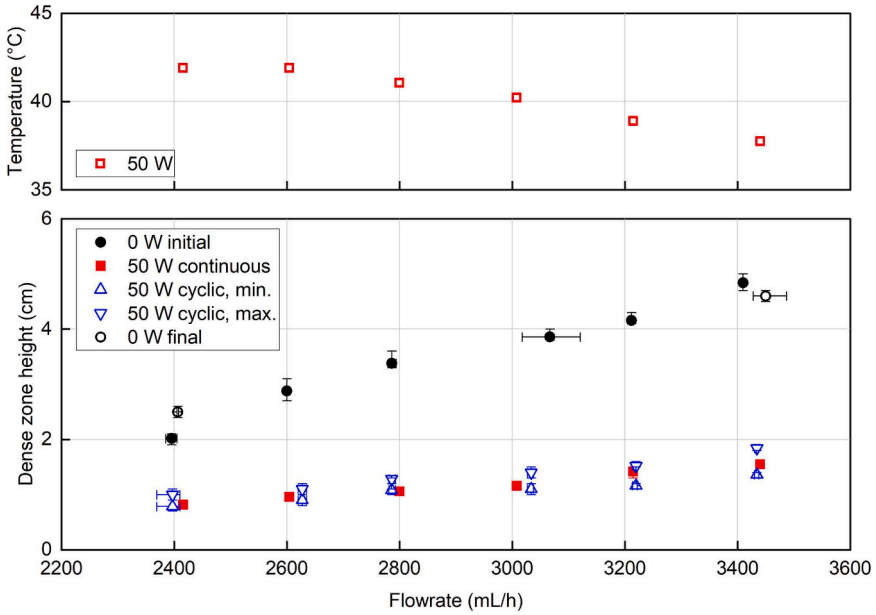

Fig. 2. Demulsification tests in a vertical settler for O/W emulsions, dense zone height in different irradiation conditions (below) and temperature under constant irradiation (above). Each symbol represents the average of six recordings under the same conditions (flowrate and microwave irradiation), the horizontal error bars represent the flowrate fluctuations during these recordings, the vertical error bars represent the lowest and highest of the dense zone height.

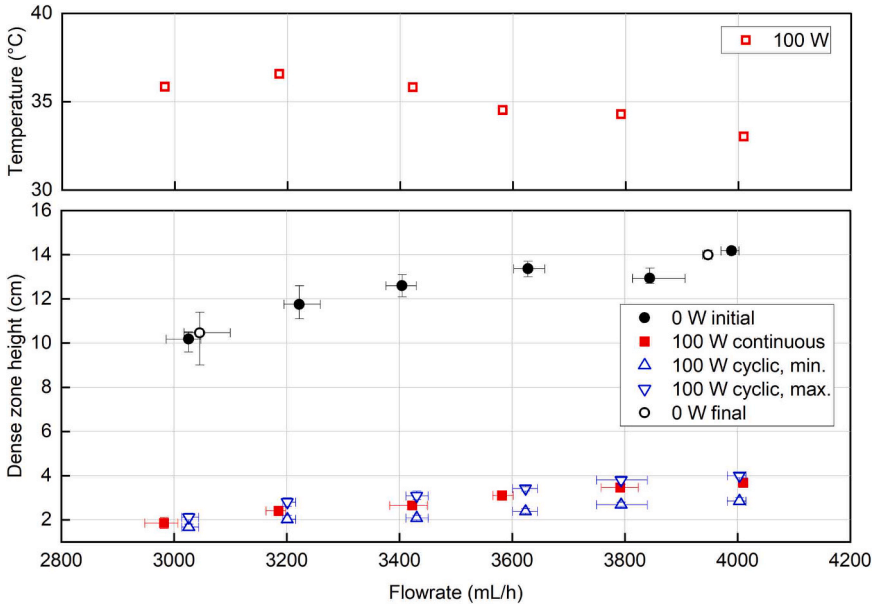

Fig. 3. Demulsification tests in a vertical settler for W/O emulsions, dense zone height in different irradiation conditions (below) and temperature under constant irradiation (above).

5.1. Permittivity measurements and modelling procedure

Three types of measurements were performed: (i) on the individual phases (after chemical equilibration with their counterpart phase because of the non-zero mutual solubility of water and TBP); (ii) on emulsions inside the stirred beaker with known phase fraction; and (iii) in dense-packed emulsions at different heights, (so with different phase fractions).

For the stirred emulsions, only 30 mL of continuous phase and 10 mL of dispersed phase were initially placed in the beaker. Each subsequent measurement was made after adding 5 mL of dispersed phase and stirring for 1 min at 5000–15000 rpm. All measurements were conducted in triplicates and the mean values were used for model fitting. The measurements were all performed at ambient temperature (21°C ± 1°C). The estimated uncertainties were less than 5 %.

For the densely packed emulsions, measurements were performed in a graduated cylinder containing 3–5 cm of the studied emulsion. The measurement process was repeated 3 times, the probe being wiped between two measurements to prevent accumulation of dispersed phase on it, possibly by favored wetting. The estimated measurement error was ± 20 % mainly due to the difficulty of reproducing identical emulsions. For permittivity measurements in the separate phases, the estimated uncertainties were less than 5 %.

Fig. 4 shows the measurement setup for dense emulsions. If the fraction of dispersed phase varies along the *z*-axis, it will also lead to variations in permittivity. Permittivity measurements were therefore

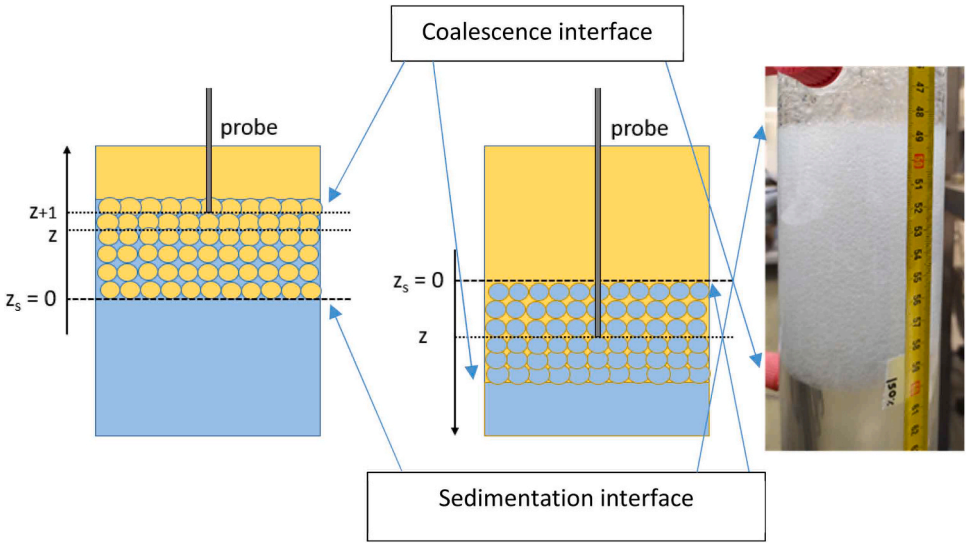

Fig. 4. Diagrams of the setup used for measurements in dense emulsions: left, aqueous continuous phase; right, organic continuous phase (droplets not to scale) and photo of the dense emulsion in organic continuous phase.

performed at several heights in the dense emulsion layer, immediately after the emulsion was formed (approximately 2 minutes after production) and a second time after the emulsion had been left to settle for ten minutes. Note that sedimentation was complete even after 2 minutes, and separate layers of respectively continuous phase, emulsion, and dispersed phase were clearly observed in the measurement cylinder.

Computation of model results, based on individual phase permittivities and phase fractions, has been carried out with a Python script, over a broad frequency range (0.5–20 GHz). The developed Python script takes a list of phase fractions and individual phase permittivities as input, and outputs an array of permittivities for the corresponding emulsions, for all phase fractions and all frequencies. The calculated data can either be used in microwave heating simulations, by extracting the permittivities at a given phase fraction, or to compare the calculated permittivities with measurements made on a real emulsion to deduce the phase fractions. A schematic of the code algorithm is given in Appendix C (Fig. C-1). Permittivities calculated with different models were compared to the experimental ones measured in the emulsions obtained in stirred beaker (for which the phase fraction is known), using the following formula:

$$err_2 = \left(\frac{\mathrm{Re}\left\{\underline{\varepsilon_{calc.}}\right\} - \mathrm{Re}\left\{\underline{\varepsilon_{mes.}}\right\}}{\mathrm{Re}\left\{\underline{\varepsilon_{mes.}}\right\}} \right)^2 + \left(\frac{Im\left\{\underline{\varepsilon_{calc.}}\right\} - Im\left\{\underline{\varepsilon_{mes.}}\right\}}{Im\left\{\underline{\varepsilon_{mes.}}\right\}} \right)^2 \quad (8)$$

and minimizing the summed error over the 251 points in the 500 MHz −20 GHz range.

5.2. Individual phases permittivities

Figs. 5 and 6 show the frequency dependence of the real and imaginary parts of the permittivities, for chosen representative aqueous and organic phases. Water and pure organics (alkane and extracting molecule) are respectively shown as a reference for aqueous and organic phases.

These results show that adding ionic species (1 M KNO_3) in the aqueous phase leads to a considerable increase in the imaginary component of the permittivity at low to intermediate frequencies. This reflects the contribution of the ionic conductivity to the imaginary component:

$$\varepsilon_{total} = \varepsilon_{bound\ charges} - j\,\sigma/\omega \quad (9)$$

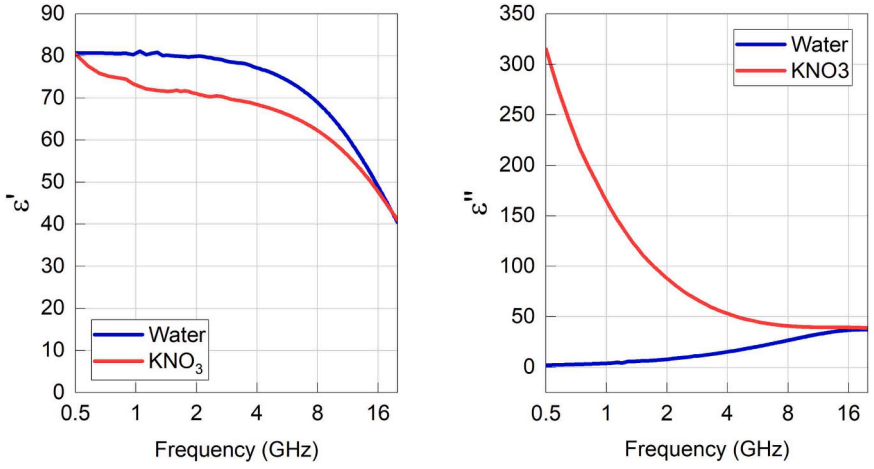

Fig. 5. Real (left) and imaginary (right) components of the relative permittivity of water (blue) and a 1 M potassium nitrate solution (red) as a function of frequency (temperature: 21°C).

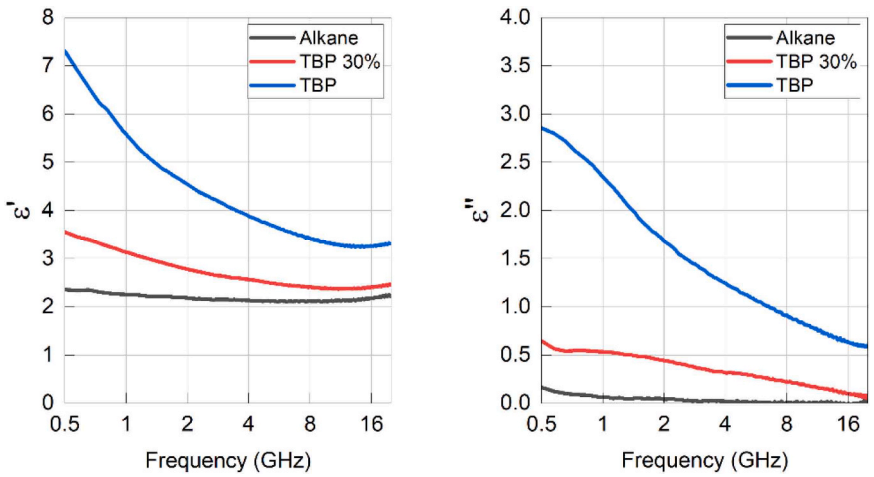

Fig. 6. Real (left) and imaginary (right) components of the relative permittivity of pure TBP (blue), pure alkane (black) and of a 30/70 % mixture of the two (red) as a function of frequency (temperature: 22°C).

where σ is the static conductivity.

As expected, the values obtained for organic phases (Fig. 6) are much lower than the ones measured on the aqueous phases. The alkane diluent shows a very low real permittivity around 2.2 and is practically lossless across the entire frequency range, while the permittivity of TBP, which is higher because its phosphate group is polar, exhibits a low frequency relaxation (around 0.5 GHz). The permittivity curve of the 30 % TBP in alkane mixture is intermediate between those of the individual components.

5.3. Permittivity of emulsions and model validation

In order to validate the models, emulsions with known phase fractions were generated (in stirred beakers) and their permittivities at 2.45 GHz were measured. Both O/W and W/O emulsions consisted of Alkane and KNO_3 1 M aqueous solution. Tiny amounts of surfactants (Tween 20, 5.10^{-5} in vol. for the continuous aqueous phase, or Span 80, at 10^{-4} in vol. for the organic continuous phase) were added to stabilize the emulsions. Fig. 7 compares the fits obtained with the Hanai, Fricke-Mudgett and Wagner models (Eqs. 5, 6 and 7) to the permittivity values measured.

The results for both emulsion types are plotted as a function of the aqueous phase fraction to highlight the different behaviors of O/W and W/O emulsions. The errors of about 20 % in the experimental data are mostly attributed to the difficulty to repeat dense emulsions preparation, leading sometimes to an inhomogeneous distribution of dispersed phase in the beaker and presence of air bubbles.

All models lead to good fits of the data for the O/W emulsions (aqueous continuous phase), which is consistent with the expectation that no additional polarization arises. For the W/O emulsions (organic continuous phase), the non-interactive Wagner and Fricke-Mudgett models fail to account for the effect of the aqueous phase when the dispersed phase fractions exceeds 0.5, particularly for the imaginary component. In contrast, the Hanai model represents the data fairly well for both types of emulsion. The Hanai model was therefore selected on this basis for the rest of the study.

5.4. Permittivity and phase fractions profiles in dense packed emulsions

The Hanai model was used to estimate the phase fractions profiles in dense emulsions, from the permittivity values measured at different heights (Fig. 4) in the setup mimicking the part of a continuous settler where the emulsion is densely packed. Each measurement was done at two or three given times (after 2, 10 and 120 minutes of settling) in the batch system, even thouth, in a real settler operating at steady state, the dense packed emulsion height is stable over time.

In this section, oil in water emulsions (continuous aqueous phase) consist in either alkane in 1 M KNO_3 at 21.5°C or 30 % TBP/alkane in 1 M KNO_3 at 21°C with no surfactant. Water in oil emulsions (continuous organic phase), consist in 1 M KNO_3 in alkane at 21°C with 10^{-3} in vol. of Span 80 as surfactant. The low stability of the firstly envisioned formulation for the water-in-oil emulsion (10^{-4} in vol. of Span 80 only) forced us to add Span 80 in quite larger concentration in order to stabilize the emulsion, generating smaller drops (and thus get slower

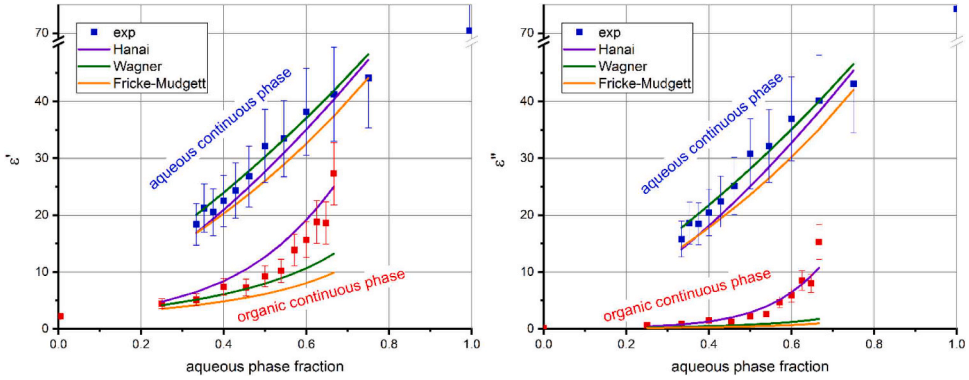

Fig. 7. Real (left) and imaginary (right) components of the relative permittivity of stirred O/W (blue) and W/O (red) emulsions at 2.45 GHz and 21°C+/1°C as a function of the aqueous phase fraction. The experimental points and error bars represent the means and estimated uncertainties of two independent series of measurements.

drainage of the continuous phase) in the process. According to prior experiments with endoscopic measurements/photographs (not shown) with a resolution of 10 μm and sedimentation times, we can estimate the smallest size to be comprise between 1 and 10 μm. The absence of influence of such amounts of surfactant on the permittivity of individual phases has been checked. The same is assumed for the permittivity of emulsions. As these emulsions drain relatively slowly, a third set of measurements was performed after 120 min. We also tried 1 M KNO_3 in 30 % TBP in alkane mixture as the continuous phase, but the latter emulsions were too unstable for permittivity measurements. It is likely that that TBP interacts with Span 80 and limits the surfactant's stabilizing effect on the interfaces.

Typical permittivity plots and Hanai's model fits are shown in Appendix D. The corresponding estimations of the phase fractions are reported in Table 1. The empty cells correspond to heights at which the emulsion was already coalesced.

Increasing dispersed phase fractions result in decreasing permittivities for O/W systems, and inversely in increasing permittivities in W/O systems (see Appendix D, Figures D-1 and D-2). In all cases, the dispersed phase fractions increase over time, as the continuous phase drains. They also increase as the measurement probe is moved closer to the coalescence interphase. The calculated phase fraction values, ranging from 0.64 to 0.90, are consistent with a dense packed zone. Above the dense packing limit (*i.e.* dispersed phase fraction of about 0.64), the droplets can no longer be both spherical and single-sized. An assembly of polydispersed spherical droplets is likely to form above the 0.64 packing threshold, with smaller drops occupying the spaces between the larger ones. Alternately, an assembly of deformed monodispersed drops can form. The fraction of dispersed phase varies along the *z*-axis as the hydrostatic and Laplace pressures balance (Verbist et al., 1996). In the studied emulsions, the drops deformed under the effects of their collective cumulative and buoyancy, while finite coalescence rate promotes the coexistence of droplets with different sizes, even if the emulsion was initially monodisperse.

As a conclusion, in industrial separation systems like liquid-liquid extraction columns, if an emulsified dense zone appears, the dispersed phase fraction will present a profile along the vertical axis, from around 0.64–0.95 as we go from well-ordered semi-rigid droplets to deformed droplets ready to coalesce. Permittivities will follow this evolution and the Hanai model is perfectly suitable to predict the permittivity profiles along the z-axis in the dense emulsion zone. This result is all the more remarkable since this model does not account for the drops size and distribution which must nevertheless have an effect on the concentration of drops at the interfaces.

5.5. Numerical simulations and scale up calculations

Numerical simulation was first used to better interpret the experimental demulsification results of Section 5 then to investigate how microwave would propagate and heat emulsions at a large industrial scale. Simulations were performed using the RF module of the COMSOL Multiphysics 6.0 simulation platform, solving the electric field propagation equation (Eq. 1) with proper boundary conditions, using the permittivity values reported in section 5.4 for both O/W and W/O emulsions. The considered outputs of the simulations were therefore the instantaneous electric field distribution and instantaneous absorbed power under the initial irradiation conditions (Eq. 2).

5.6. Cylinder geometry at laboratory scale

Numerical simulations were performed inside a rectangular cavity filled with air, the dimensions of which are those of the experimental standard WR340 waveguide (86.36 mm×43.18 mm). A piston is placed at one end of the device, for power matching between the sample and the microwave generator. A cylinder, mimicking the dense zone of the experimental laboratory column, is placed at the heart of the cavity, crossing the trajectory of the waveguide (Fig. 8). The cylinder is filled with the most stable emulsions, namely alkane in KNO_3 solution (dispersed phase fraction, 0.90) for the O/W system and KNO_3 solution in alkane (dispersed phase fraction, 0.72) for the O/W system.

The medium is considered homogeneous and the permittivities values obtained in section 5.4 are used. The incident power was set to 50 W, but the results can be transposed to any power value, since the spatial distributions of the electric field and absorbed power do not depend on the incident power (only the magnitudes do). Several cylinder radii were considered, ranging from 0.5 to and 2 cm. The position of the piston was also varied by more than half the wavelength. In each case, the holdup (hence the permittivity) of the emulsion is supposed constant, but the model can also handle variable emulsion properties, thanks to the Hanai model, providing the coalescence kinetics is known.

Fig. 9 compares the electric field intensity in the two types of emulsion. The effect of the cylinder diameter is shown in Fig. 10. Table 2 lists the maximum absorbed power, expressed as a percentage of the incident one, in all the configurations considered (considering that the load of the microwave system is optimized by moving the piston or by other means such as stubs.)

Because of its high permittivity, the KNO_3-in-alkane emulsion prevents the electric field from propagating to the right side of the

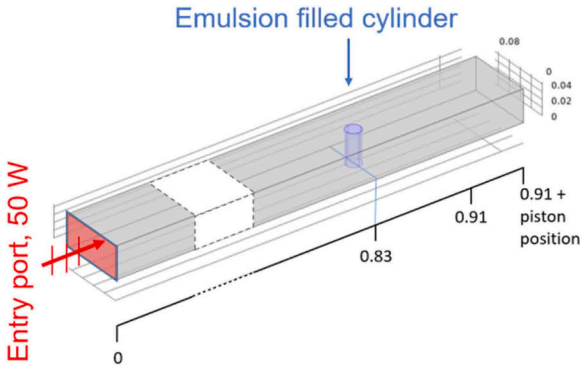

Fig. 8. Schematic diagram of the simulated setup with an emulsion-filled cylinder placed inside a waveguide.

Table 1
Fitted phase fractions (Hanai model) at different heights in oil-in-water emulsions.

	Oil in Water (with no surfactant)				Water in Oil (with Span80 10^{-3} in vol.)		
	Alkane / KNO_3		30 %TBP-70 %alkane / KNO_3		KNO_3 / alkane		
Height	Φ at 2 min.	Φ at 10 min.	Φ at 2 min.	Φ at 10 min.	Φ at 2 min.	Φ at 10 min.	Φ at 120 min.
0 cm	0.57	0.68	0.71	0.74	0.22	0.34	0.67
Sedimentation interface							
1 cm	0.64	0.82	0.79	0.81	0.31	0.42	0.87
2 cm	0.75	0.96	0.80	0.83	0.35	0.53	0.92
3 cm	0.83	-	0.83	0.88	0.48	0.67	0.83
4 cm	0.91	-	0.85	0.90	0.60	0.72	0.94
Towards coalescence interface							

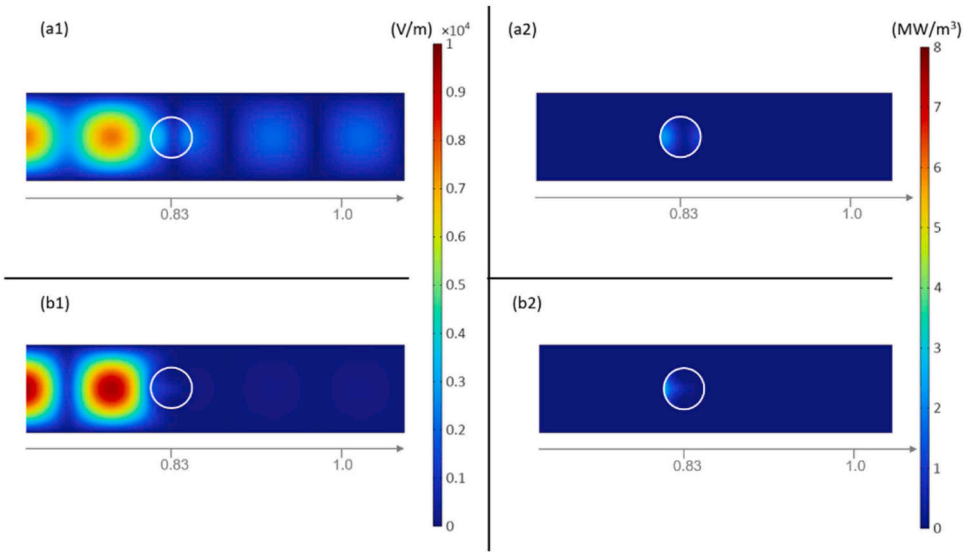

Fig. 9. Electric field (left) and dissipated power (right) distributions inside the waveguide for (a) alkane in KNO_3 and (b) KNO_3 in alkane emulsions. Cylinder radius, 0.02 m.

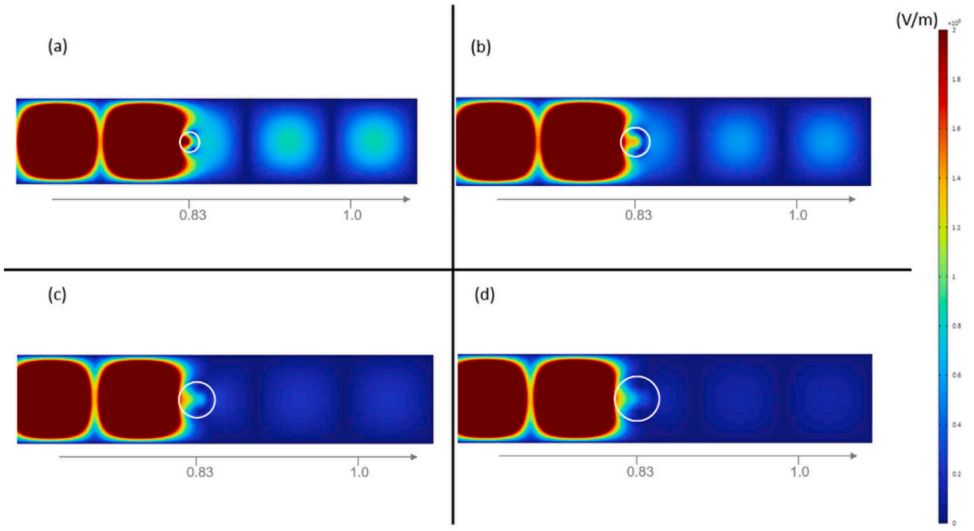

Fig. 10. Effect of the cylinder radius. Electric field distributions inside a waveguide containing a $KN0_3$-in-alkane emulsion ($\Phi = 0.72$) inside a cylinder of radius (a) 0.01 m, (b) 0.014 m, (c) 0.018 m, and (d) 0.022 m. The maximum of the color scale is 2 kV/m.

Table 2
Fractions (in %) of the incident power absorbed by the emulsions at optimal piston lengths for different cylinder radii.

	Cylinder radius			
	0.5 cm	**1 cm**	**1.5 cm**	**2 cm**
Alkane / KNO_3 ($\Phi = 0.9$) $\varepsilon' = 4.99$ $\varepsilon'' = 2.49$	80.8 %	98.8 %	95.8 %	84.2 %
KNO_3 / alkane ($\Phi = 0.72$) $\varepsilon' = 26.92$ $\varepsilon'' = 14.74$	46.0 %	55.8 %	46.8 %	43.6 %

waveguide (Fig. 9b), despite being contained in a relatively small cylinder. Since none of the radiation reaches the piston, moving the piston has no effect on the absorbed power. This result highlights the fact that the optimal setup to maximize the absorbed power depends strongly on the properties of the emulsion. For alkane-in-KNO_3, the microwaves propagate through the sample (Fig. 9a) and more power is absorbed because of the higher dispersed phase fraction and lower permittivity compared with the KNO_3-in-alkane emulsion (Table 2). The absorbed power at the optimal piston position ranges from 80.8 % to 98.8 % of the input power, depending on the diameter of the cylinder. Fig. 10 shows that larger cylinders prevent the electric field from propagating beyond the sample, reducing the level of power matching than can be achieved by moving the piston. Overall, samples that are too lossy too large prevent the electric field from propagating inside the whole cavity and thereby limit the load matching effect of the piston.

These simulation results are fully consistent with the experiment observations of Section 5: regardless of the emulsion direction (W/O or O/W), microwaves propagate in the system, where they convert into heat, thus leading to a better drainage of the continuous phase and a favored coalescence of the droplets, achieving the emulsion collapse in both configurations. The electric field and the dissipated power mainly locate on the left side of the tubes, ie upstream the tube (Figs. 9 and 10), which seems to indicate that the temperature is not uniform in the cylinder. Although a local increase in temperature is likely to cause a dissymmetric collapse of the emulsion, the void created will be immediately filled by the surrounding emulsion.

Finally, the diameter of the cylinder is an additional parameter which can be optimized.

5.7. Semi-infinite waveguide

Since the ultimate goal of this work is to discuss the relevance of implementing microwave demulsification in a continuous industrial settler, we decided to investigate how the variations in the permittivity of W/O and O/W emulsions affect the propagation of electric fields and heat dissipation patterns inside a large volume. In the following simulations, emulsions occupy the whole section of the WR340 waveguide past the 0.8 m mark (see Fig. 11). The thickness of the sample (30 cm) was chosen far above the anticipated penetration depth to minimize the effects of reflected waves travelling back along the guide and complicating the readings of wavelengths and penetration depths. The incident power was again set to 50 W for simulations. Fig. 11 shows the magnitude of the electric field along the waveguide centerline with both modes of emulsion (W/O and O/W described in Table 2- column 1).

A drastic change in wavelength between the empty waveguide ($x < 0.8$ m) and the part filled with emulsion ($x > 0.8$ m) is observed. Successive zeros or maxima are one half-wavelength apart, giving wavelengths in air, in the O/W emulsion and in the W/O emulsion of 17.35 cm, 5.59 cm and 2.3 cm respectively, with corresponding penetration depths of 3.44 cm inside the alkane-in-KNO_3 emulsion and 1.40 cm in the KNO_3-in-alkane emulsion, calculated from the ratio of the electric field between two consecutive maxima inside the material from:

$$\left|\frac{E(x)}{E\left(x-\frac{\lambda}{2}\right)}\right| = e^{\frac{-\lambda}{2d_p}} \tag{10}$$

The total dissipated power is 35.5 W and 19.6 W respectively.

Because of its higher water and ion content, the W/O emulsion has a higher reflection coefficient and absorbs less power, as the microwaves are more strongly attenuated and have a shorter wavelength. However, for both types of emulsion, a heating of a few centimeters width, is achieved under microwave irradiation.

5.8. Scale-up calculations and guidelines

Considering the above results, the heating effect in both types of emulsions should be sufficient to trigger demulsification. For the KNO_3-in-alkane emulsion, reflection losses could easily be minimized by adding tuning elements between the power source and the sample. The short penetration depth inside emulsions with high ionic contents means that relatively small zones can be treated in this way. Consequently, a narrow column roughly 2 or 3 cm in diameter can perfectly be used to study coalescence under microwave heating on a laboratory scale. Larger columns can be designed anyway because the local collapse of an emulsion will be followed by the immediate filling of the created void and rapidly the collapse of the whole emulsion.

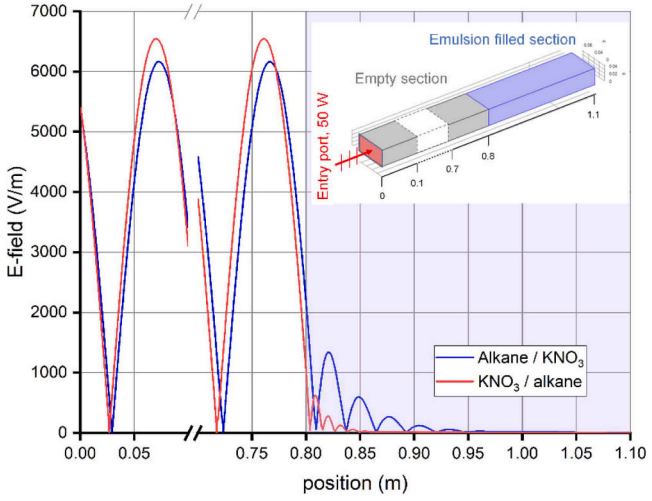

Fig. 11. Instantaneous electric field magnitude as a function of distance along the center of the waveguide shown in the inset. The part of the graph corresponding to the emulsion-filled region is shaded in blue.

The wide frequency range investigated for permittivities can be used to calculate the wavelengths and penetration depths inside the emulsions at various ISM frequencies (frequencies reserved for Industrial, Scientific and Medical use, as opposed to communication frequencies) such as 5.8 GHz, 2.45 GHz and 915 MHz (Table 3). Wavelengths and penetration depths are given by Eqs. 3 and 4.

The penetration depths and wavelengths logically increase when frequency decreases reaching several centimeters values. This suggest however that this limitation could be offset by reducing the microwave frequency. Furthermore, heating just the first few centimeters of a dense emulsion may be sufficient to destabilize and eventually collapse the entire dense zone by a redistributive effect, as the rest of the emulsion would come to occupy the vacant space near the walls and thus be exposed to microwave radiation. Circulation of the continuous phase (not included in this work) should also help, in creating additional convective movement.

5.9. Economic viability

The economic viability of such microwave intensified processes is often the evoked barrier preventing their industrial application. But this argument only applies if we simply compare the CAPEX and OPEX of microwave heating with other conventional heating techniques. If the cost of one magnetron and its associated piloting equipment is clearly superior to that of a heating resistor, microwave technology brings indirect benefits making maintenance much easier and safer for staff. In the nuclear industry, maintenance is a big fraction of costs and an even bigger fraction of personnel exposition: reducing maintenance need, close to the fluids, thanks to microwaves ability to heat from a distance, could reduce worker exposition and associated costs. No other heating technique can keep the heating elements away from radioactive areas. The fast dynamics of microwave heating also enhance process safety, again providing socio-economic benefits. In addition, one wave generating element could be employed to power multiple microwave enhanced settler stages in extractor batteries, which are common in the industry, thanks to appropriate waveguide geometries. Finally, it should be noted that “radio frequency desalters” are already employed in the petroleum industry, to separate brine droplets from petroleum, hinting at a possible application of microwaves in the same manner. Even if no financial full study is available, the advantages of microwave heating as a phase separation intensification method can obviously justify its downrange socio-economic viability.

6. Conclusion

The demulsification of liquid-liquid systems for metal recycling by microwaves has been experimentally demonstrated in this study. Despite the high conductivity of the ionic aqueous phases industrially used and the specific characteristics of the organic phases, very fast microwave demulsification is achieved in both W/O and O/W emulsions. The dielectric properties of these representative emulsions have been measured and modeled and the Hanai model was chosen as the most accurate for calculating the permittivity of emulsions using the permittivities measured in the separate phases and the phase fractions. This allows permittivities to be estimated over a wide range of frequencies, along with microwave penetration depths at different phase fractions. Numerical simulations of the electric field distribution and penetration depths calculations at several frequencies demonstrate that

Table 3
Relative permittivity of the studied liquids and emulsions at 5.8 GHz, 2,45 GHz and 915 MHz and the corresponding wavelengths and microwave penetration depths.

Frequency	5.8 GHz				2.45 GHz				915 MHz			
	ε'	ε''	λ (cm)	d_p (cm)	ε'	ε''	λ (cm)	d_p (cm)	ε'	ε''	λ (cm)	d_p (cm)
KNO_3 1 M, 26.7°C	65.85	44.55	0.61	0.32	70.43	74.25	1.32	0.49	74.12	179.21	2.83	0.67
30 %TBP – 70 %alkane, 22.3°C	2.47	0.28	3.29	9.40	2.70	0.41	7.42	15.86	3.19	0.54	18.28	34.73
Alkane / KNO_3, 21°C Φ=0.90	4.59	1.52	2.38	2.34	4.99	2.49	5.32	3.60	5.43	5.87	12.66	4.60
KNO_3 / alkane, 21°C Φ=0.72	24.15	9.92	1.03	0.83	26.92	14.74	2.28	1.42	35.12	30.82	5.13	2.17

microwave heating is relevant and possible in both W/O and O/W dense packed emulsions, which should rapidly lead to demulsification even at industrial scale. Finally, the results of this study are the first steps toward the design of microwave intensified liquid-liquid separators.

CRediT authorship contribution statement

Isabelle Polaert: Conceptualization, Formal analysis, Funding acquisition, Investigation, Methodology, Project administration, Supervision, Validation, Writing – original draft, Writing – review & editing. **Lionel Estel**: Conceptualization, Investigation, Methodology, Supervision, Validation. **Sophie Charton**: Conceptualization, Funding acquisition, Validation, Writing – original draft, Writing – review & editing. **Clelio Cerino**: Data curation, Formal analysis, Investigation, Methodology, Writing – original draft. **Hervé Roussel**: Data curation, Formal analysis, Investigation, Methodology, Writing – original draft, Writing – review & editing.

Declaration of Competing Interest

The authors declare that they have no known competing financial interests or personal relationships that could have appeared to influence the work reported in this paper

Acknowledgements

This work was financially supported by the Energy Division of CEA (PRATA Program).

The authors thank Fabrice Lamadie from CEA Marcoule for his valuable help in measuring the drop-size distribution in the perforated plate experiment.

Appendix A. drop size in the perforated plate vertical settler

Drop size was measured by means of backlight ombroscopy. A settler similar to that used in microwave experiments was used, fitted with two flat viewing windows to allow illumination and image capture without optical distortion. The drops were photographed in the low retention zone, between the perforated plate and the dense emulsion zone. Image analysis was used to calculate the size distribution of the droplet population, using an in-house developed algorithm. This measurement was carried out in W/O mode for different flow rates, corresponding to the flow rates of the microwave tests. It shows that the size of the drops is very narrow around an average value slightly smaller than the diameter of the holes (0.5 mm).

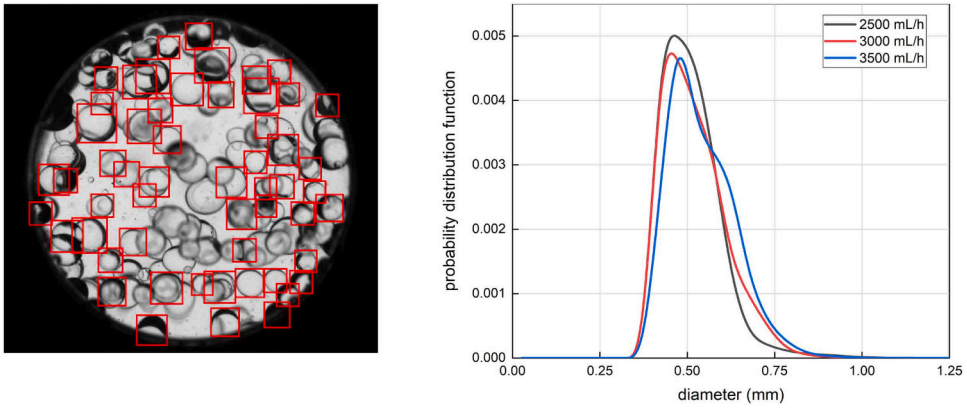

Figure A-1. image of the emulsion with the automatically detected droplets (left), drop size distribution at various flowrates (right).

Appendix B. emulsion formation

Two different ways of producing emulsions were employed. Stirred emulsions were produced directly inside a 100 mL beaker, using a modified IKA T-18 Ultra-Turrax disperser (the stator was removed to maximize entrainment, at the expense of shearing power). The disperser was equipped with an S 18 D - 10 G – KS plastic head (6.75 mm toothed rotor diameter), and was operated between 5000 and 15000 rpm, depending on the power required to agitate the whole beaker. Dispersed phase was added progressively with a burette.

Dense emulsions were produced using a Micropore LDC-1 dispersion cell (Fig. A-1), modified to operate in continuous mode by adding two input/output ports, one to add the continuous phase and the other to extract the emulsion. Droplets ranging from 200 to 300 μm in diameter were generated using steel membranes with 40 μm holes, employing a hydrophobically-treated membrane for W/O emulsions. In this device, the dispersed phase is pumped through the appropriate membrane, and a stirrer blade in the continuous phase generates a shear at the surface of the membrane, detaching the drops.

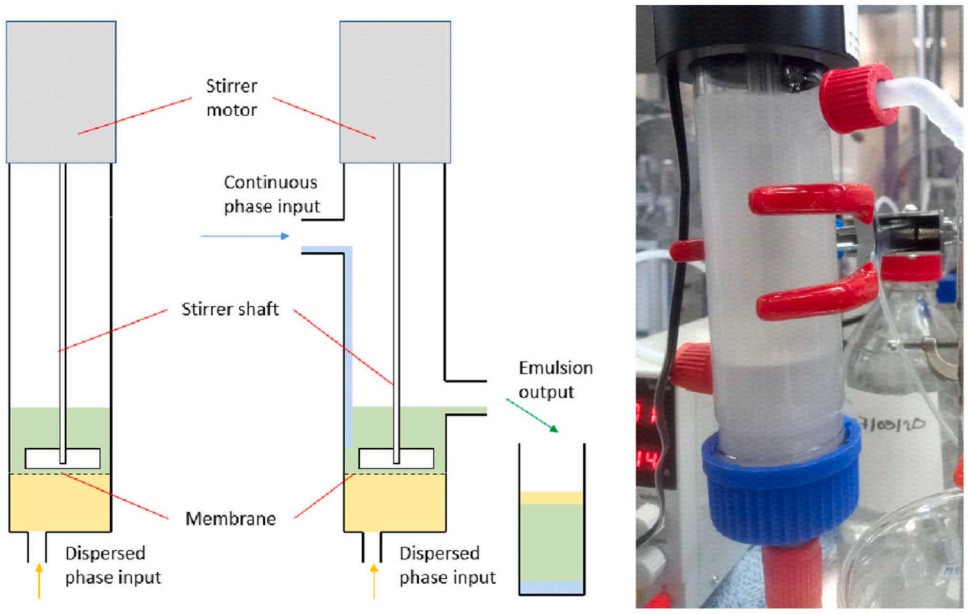

Figure B-1. Diagrams (left, center) and photograph (right) of a Micropore LDC-1 dispersion cell in the original setup (left) or modified for continuous use (center, right).

For batch emulsion permittivity measurements, the LDC-1 emulsification chamber overflowed directly into a 100 mL measuring cylinder (4 cm diameter approximatively). This system allows the formation of a thick, vertical spanning dense-packed zone where measurements are performed at different heights.

Appendix C. emulsion permittivities calculation algorithm

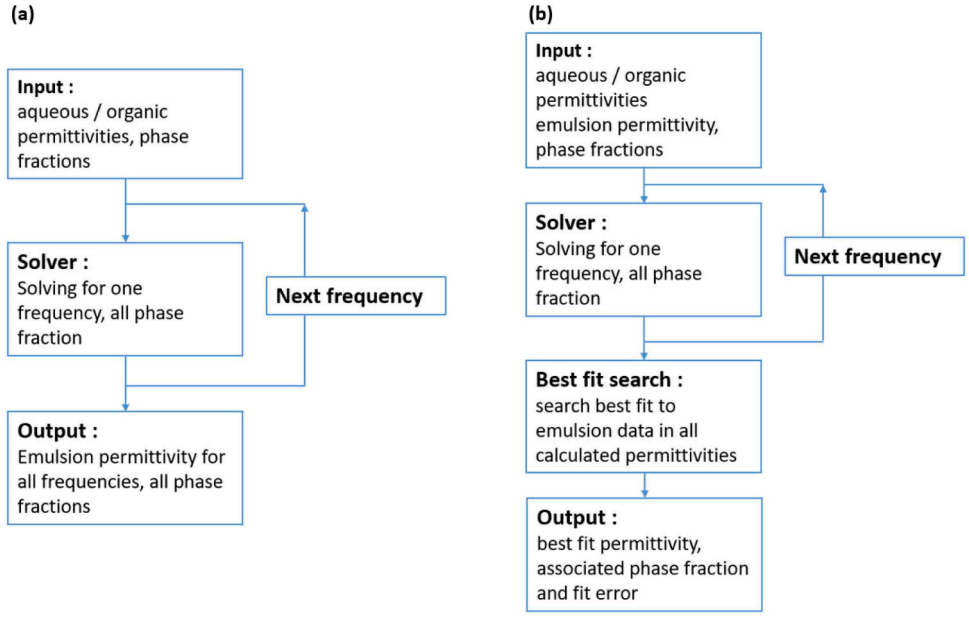

Figure C-1. Schematic representation of the Python fitting algorithm: (a) direct calculation, (b) phase fraction optimization as proposed by Thomas (Thomas, C., Perl, J. P. & Wasan, D. T., 1990).

Appendix D. experimental and calculated permittivities in the dense packed emulsions experiments

Fig. D-1 and Fig. D-2 respectively show the real and imaginary components of the permittivity of an O/W emulsion with a 30/70 % TBP/alkane mixture dispersed in 1 M KNO_3 1 M, and an W/O emulsion consisting of 1 M KNO_3 dispersed in pure Alkane. The values obtained at different measurement heights are shown along with fits of the experimental data using the Hanai model. The fitted phase fractions are reported in Table 3.

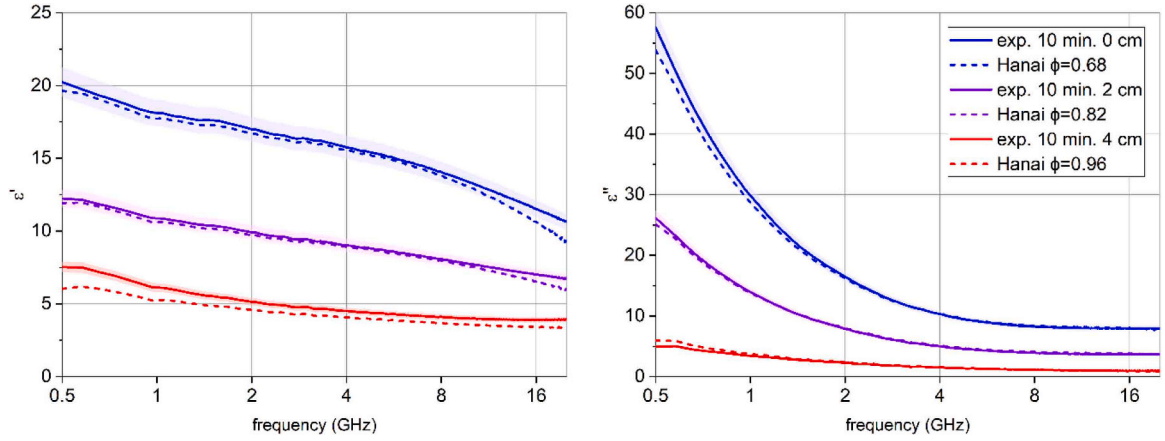

Figure D-1. Real (left) and imaginary (right) components of the relative permittivity of a 30/70 % TBP/alkane-in-KNO_3 emulsion as a function of frequency. The three solid curves correspond to measurements at different heights (blue, 0 cm; purple, 2 cm; red, 4 cm) and the dashed lines are fits with the Hanai model.

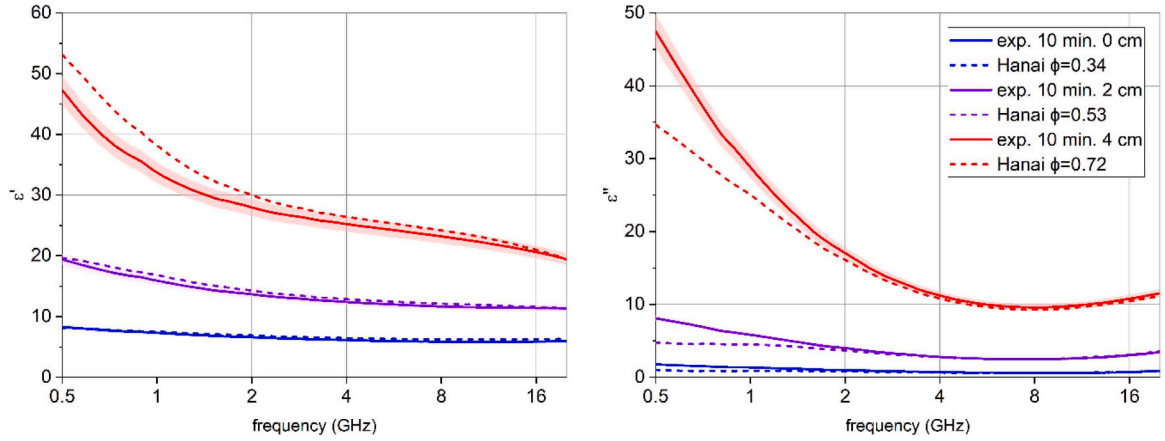

Figure D-2. Real (left) and imaginary (right) components of the relative permittivity of a KNO3-in-alkane emulsion as a function of frequency. The three solid curves correspond to measurements at different heights (blue, 0 cm; purple, 2 cm; red, 4 cm) and the dashed lines are fits with the Hanai model.

References

Baker, A., Fells, A., Carrot, M., Maher, C.J., Hanson, B., 2022. Process intensification of element extraction. Chem. Soc. Rev. 51, 3964.

Binner, E.R., Robinson, J.P., Silvester, S.A., Kingman, S.W., Lester, E.H., 2013. Separation of oil: water emulsions in continuous flow using microwave heating. Energy Fuel 27, 3173.

Binner, E.R., Robinson, J.P., Silvester, S.A., Kingman, S.W., Lester, E.H., 2014. Investigation into the mechanism by wich microwave heating enhances separation of water-in-oil emulsions. Fuel 116, 516.

Bostock, T., Boyle, M., McDonald, M., Wood, R., 1980. The dielectric behavior of nonionic micellar and microemulsion systems. J. Colloids Interface Sci. 73 (2), 368–372.

Chan, C., Chen, Y., 2002. Demulsification of W/O emulsion by microwave radiation. Sep. Sci. Technol. 3407.

Deminière, B., Colin, A., Leal-Calderon, F.B., 1998. Coarsening due to coalescence and life-time of concentrated emulsions. Comptes Rendus De. l'Acad. émie Des. Sci. - IIC - Chem. 1, 163–165.

Epstein, B., Foster, K., Mackay, R., 1983. Microwave dielectric properties of ionic and nonionic microemulsions. J. Colloid Interface Sci. 95 (1), 218–227.

Erle, U., Regier, M., Persch, C., Schubert, H., 2000. Dielectric properties of emulsions and suspensions: mixture equations and measurement comparisons. J. Microw. Power Electromagn. Energy 35 (3), 185.

Estel, L., Poux, M., Benamara, N., Polaert, I., 2017. Continuous flow-microwave reactor: where are we ? Chem. Eng. Process.: Process.Intensif. 113, 56–64.

Fang, C., Chang, B., Lai, P., Klaila, W., 1988. Microwave demulsification. Chem. Eng. Commun. 73.

Fang, C., Lai, P., Chang, B., Klaila, W., 1989. Oil recovery and watse reduction by microwave radiation. Environ. Prog. 8 (4), 235.

Ferreira, B., Ramalho, J., Lucas, E., 2013. Demulsification of water-in-crude oil emulsions by microwave radiation: effect of aging, demulsifier addition, and selective heating. Energy fuels 27, 615.

Fortuny, M., Oliveira, C., Melo, L., Nele, M., Coutinho, R., Santos, A., 2007. Effect of salinity, temperature, water content, and pH on the microwave demulsification of crude oil emulsions. Energy fuels 21, 1358.

Foster, K., Epstein, B., Jenin, P., Mackay, R., 1981. Dielectric studies on nonionic microemulsions. J. Colloid Interface Sci. 88 (1).

Frising, T., Noïk, C. & Dalmazzone, C. (2006). The liquid/liquid sedimentation process, from droplet coalescence to technologically enhanced water/oil emulsion gravity separator: a review. Journal of dispersion science and technology, 1035.

Han, Y., He, L., Luo, X., Lü, Y.S., Chen, J., Huang, X., 2017. A review of the recent advance in design of corrugated plate packs applied for oil-water separation. J. Ind. Eng. Chem. 53, 37–50.

Hanai, T., 1960. Theory of dielectric dispersion due to interfacial polarisation and its application to emulsions. Kolloid Z. 171 (1), 23.

Kopriwa, N. (2013). Quantitative Beschreibung von Koaleszenzvorgängen in Extraktionskolonnen, PhD, Fakultät für Maschinenwesen der Rheinisch-Westfälischen Technischen Hochschule, Aachen, 06.17.2013.

Kovaleva, L., Minnigalimov, R. & Zinnatullin, R. (2011). Destruction of Water-in-Oil Emulsions in Radio-Frequency and Microwave Electromagnetic Fields. Energy and fuels, 3731.

Lichtenecker, K., Rother, I., 1931. Die Herleitung des logaritmischen Mischungsgestezes aus allgemeinen Prinzipien der stationären Strömung. Phys. Z. 32, 255–260.

Maxwell, J. (1892). Electricity and Magnetism. London.

Mudgett, R., Wang, D., Goldblith, S., 1974. Prediction of dielectric properties in oil-water and alcohol-water mixtures at 3,000 MHz, 25°C based on pure component properties. J. Food Sci. 39, 632–635.

Pozar, D., 2012. Microwave Engineering - 4th Edition. John Wiley and Sons, Inc, Kendallville.

Rayleigh, 1892. On the influence of obstacles arranged in rectangular order upon the properties of a medium. Philos. Mag. 34, 481.

Sjöblom, J., Gestblom, B., 1986. A dielectric spectroscopic study of some ionic and nonionic microemulsions. J. F. Colloid Interface Sci. 115 (2), 535–544.

Thomas, C., Perl, J.P., Wasan, D.T., 1990. Complex dielectric properties of macroemulsions in the microwave region. J. Colloid Interface Sci. 139 (1).

Vafajoo, L., Ganjian, K., Fattahi, M., 2012. Influence of key parameters on crude oil desalting: an experimental. J. Pet. Sci. Eng. 107–111.

Verbist, G., Weaire, D., Kraynik, A., 1996. The foam drainage equation. J. Phys.: Condens. Matter 3715.
Wagner, K. (1914). Arch. Electrotechnic, 2, 371.
Ye, S., Hohl, L., Charlafti, E., Jin, Z., Kraume, M., 2023. Effect of temperature on mixing and separation of stirred liquid/liquid. Chem. Eng. Sci. 274.